Received: 12 September 2018 | Revised: 21 November 2018 | Accepted: 11 December 2018

DOI: 10.1002/mrm.27651

FULL PAPER

Magnetic Resonance in Medicine

Measuring large lipid droplet sizes by probing restricted lipid diffusion effects with diffusion-weighted MRS at 3T

Dominik Weidlich[1] | Julius Honecker[2] | Oliver Gmach[3] | Mingming Wu[1] | Rainer Burgkart[4] | Stefan Ruschke[1] | Daniela Franz[1] | Bjoern H. Menze[5] | Thomas Skurk[2] | Hans Hauner[2] | Ulrich Kulozik[3] | Dimitrios C. Karampinos[1]

[1]Department of Diagnostic and Interventional Radiology, Technical University of Munich, Munich, Germany

[2]Else Kröner Fresenius Center for Nutritional Medicine, Technical University of Munich, Munich, Germany

[3]Chair for Food and Bioprocess Engineering, Technical University of Munich, Freising, Germany

[4]Clinic of Orthopaedic Surgery, Klinikum rechts der Isar, Technical University of Munich, Munich, Germany

[5]Department of Computer Science, Technical University of Munich, Munich, Germany

Correspondence
Dominik Weidlich, Department of Diagnostic and Interventional Radiology, Klinikum rechts der Isar, Technical University of Munich, Ismaninger Str. 22, 81675 Munich, Germany.
Email: dominik.weidlich@tum.de

Funding information
European Research Council, Grant/Award Number: 677661 (ProFatMRI); Philips Healthcare

Purpose: The in vivo probing of restricted diffusion effects in large lipid droplets on a clinical MR scanner remains a major challenge due to the need for high b-values and long diffusion times. This work proposes a methodology to probe mean lipid droplet sizes using diffusion-weighted MRS (DW-MRS) at 3T.

Methods: An analytical expression for restricted diffusion was used. Simulations were performed to evaluate the noise performance and the influence of particle size distribution. To validate the method, oil-in-water emulsions were prepared and examined using DW-MRS, laser deflection and light microscopy. The tibia bone marrow was scanned in volunteers to test the method repeatability and characterize microstructural differences at different locations.

Results: The simulations showed accurate and precise droplet size estimation when a sufficient SNR is reached with minor dependence on the size distribution. In phantoms, a good correlation between the measured droplet sizes by DW-MRS and by laser deflection ($R^2 = 0.98$; $P = 0.01$) and microscopy ($R^2 = 0.99$; $P < 0.01$) measurements was obtained. A mean coefficient of variation of 11.5 % was found for the lipid droplet diameter in vivo. The average diameter was smaller at a proximal (50.1 ± 7.3 μm) compared with a distal tibia location (61.1 ± 6.8 μm) ($P < 0.01$).

Conclusion: The presented methods were able to probe restricted diffusion effects in lipid droplets using DW-MRS and to estimate lipid droplet size. The methodology was validated using phantoms and the in vivo feasibility in bone marrow was shown based on a good repeatability and findings in agreement with literature.

KEYWORDS
adipocytes diameter, adipose tissue microstructure, diffusion of fat, DW-MRS, lipid droplet

[Correction added after online publication January 23, 2019: The authors have corrected an error in the Funding Information and edited the Acknowledgment in this version].

1 | INTRODUCTION

The measurement of lipid droplet size is important in the study of adipose tissue and ectopic lipids in both health and metabolic dysfunction across organs and tissues. In skeletal muscle, droplets of intramyocellular lipids are significantly smaller than extramyocelluar lipid droplets.[1] In fat depots containing brown adipose tissue, brown adipocytes consist of much smaller lipid droplets than white adipocytes.[2] In white adipose tissue, the adipocyte size has long been known to relate to the obese phenotype.[3] In bone marrow, adipocyte size has been recently linked to the differentiation of constitutive marrow adipose tissue from regulated marrow adipose tissue.[4] Therefore, the assessment of lipid droplet size enables the measurement of ectopic lipid droplet size (e.g., in intramyocellular lipids), the measurement of adipocyte size in adipocytes containing unilocular lipid droplets (e.g., in white adipocytes and bone marrow adipocytes), and the differentiation between adipocytes containing small multilocular lipid droplets (brown adipocytes) from large unilocular lipid droplets (white adipocytes). However, such an assessment of lipid droplet size in tissue currently requires a highly invasive biopsy procedure.

Diffusion-weighted (DW) MR is a powerful tool for the noninvasive assessment of tissue microstructure. The reduction of the ADC with increasing diffusion times due to diffusion restriction effects has been previously applied to extract cell size in vivo in water-containing tissues.[5] Measuring the diffusion properties of lipids has proven to be more challenging because fat has a diffusion coefficient approximately 2 orders of magnitude lower than water due to the large molecular size of fatty acids.[6,7] The low lipid diffusion coefficient increases the required diffusion encoding strength and diffusion time. The requirement for strong diffusion encoding and long diffusion times induces additional technical challenges related to eddy currents[8] and an overall increased sensitivity to any type of physiological tissue motion including involuntary movement.[9] Furthermore, the spectral complexity of fat (the fact that fat is composed of multiple fat peaks) constitutes a major challenge in the acquisition of DW-MR imaging measurements in fatty tissues.[10]

DW-MRS is a versatile tool to measure the diffusion properties of metabolites other than water.[11,12] When a high b-value is applied to fatty tissues, DW-MRS can measure the diffusion properties of lipids while additionally resolving the different fat peaks.[6] Recently, a high b-value DW-MRS has been applied to study myocellular lipid diffusion[13] and to quantify the intramyocellular lipid droplet size by analyzing the ADC dependence on diffusion time.[14] Diffusion restriction effects on the dependence of the DW signal on b-value have also been reported in murine brown adipocytes ex vivo using a preclinical MR system with strong magnetic field gradients.[15] Murine brown adipocytes enclose many lipid droplets with a diameter below 10 μm, whereas white adipocytes enclose a single lipid droplet with diameters between 50 and 150 μm. In white adipocytes, the size of a lipid droplet would be equivalent to the size of an adipocyte. Diffusion restriction effects are visible in the signal decay curves when molecules do not freely diffuse but hit a diffusion restricting barrier during the diffusion sensitizing period of time. The larger the dimensions of the restricting barriers in comparison to the mean free path diffusion length the smaller the measurable effect is. Therefore, the sensitization of diffusion restriction effects in white adipocytes requires long diffusion times.

Presently, DW-MRS is yet to be applied for the noninvasive measurements of lipid droplet size in large cells such as white adipocytes or bone marrow adipocytes. Probing diffusion restriction effects in large lipid droplets in vivo at a clinical scanner remains a major technical challenge due to the need for high b-value and long diffusion time DW-MRS and the sensitivity to macroscopic motion effects. The present work proposes a methodology to probe diffusion restriction effects in large lipid droplets using DW-MRS at a clinical 3T system. The bone marrow region of the lower leg has been selected as a tissue minimally affected by physiological motion effects to show the in vivo feasibility of the lipid droplet size measurements. The proposed method was first evaluated using simulations, was validated experimentally in water–fat phantoms, and then was finally applied in vivo to estimate the bone marrow adipocyte size within the tibia bone of healthy subjects.

2 | METHODS

2.1 | Theoretical background

Diffusion restriction barriers in an MR experiment will introduce deviations from the monoexponential signal decay and a reduction of the ADC values with increasing diffusion time. Assuming spherical boundaries, Murday and Cotts described the diffusion signal decay curve when restricted diffusion occurs[16]:

$$\ln\left(\frac{S(\Delta,\delta,G)}{S_0(\Delta)}\right) = -2\gamma^2 G^2 \sum_{m=1}^{\infty}\left[\alpha_m^2\left(\alpha_m^2\left(\frac{d}{2}\right)^2 - 2\right)\right]^{-1} * \left(\frac{2\delta}{\alpha_m^2 D} - \frac{2+\exp(-\alpha_m^2 D(\Delta-\delta)) - 2\exp(-\alpha_m^2 D\delta) - 2\exp(-\alpha_m^2 D\Delta) + \exp(-\alpha_m^2 D(\Delta+\delta))}{(\alpha_m^2 D)^2}\right) \quad (1)$$

where S is the DW signal, S_0 is the signal weighted by spin density and relaxation effects, Δ is the diffusion time, δ is the diffusion gradient length, G is the gradient strength, γ is the gyromagnetic moment, d is the diameter of the spherical restriction barrier, D is the free diffusion constant, and α_m are the roots obtained by the following differential equation of Bessel functions:

$$\left(\alpha_m \frac{d}{2}\right) J'_{\frac{3}{2}}\left(\alpha_m \frac{d}{2}\right) - \frac{1}{2} J_{\frac{3}{2}}\left(\alpha_m \frac{d}{2}\right) = 0 \quad (2)$$

The equation for signal attenuation (Equation 1) is not only a function of the b-value and the diffusion constant but also a function of the diffusion time and the diameter of the diffusion restricting spheres. Therefore, the size of the diffusion restricting barriers can be extracted based on the DW signal at different diffusion times and diffusion weightings as shown in Equation 1.

2.2 | DW-MRS pulse sequence and spectra postprocessing

To measure the diffusion properties of lipids, a bipolar DW STEAM MRS (Figure 1) sequence was used. The sequence was based on a standard STEAM with additional diffusion gradients in all 3 axes added after the first and third RF pulse to induce diffusion weighting.[17] The diffusion gradient duration was maximized for a given TE and the strength of the diffusion weighting gradients was adjusted to achieve certain b-values. The readout started right after the second diffusion sensitizing gradient. The mixing time was increased while keeping the b-value constant to achieve the same diffusion weighting at different diffusion times. The DW spectra with different polarity of the DW spectra were acquired to compensate for eddy-current effects (half of the averages were acquired with positive and the other half with negative polarity).

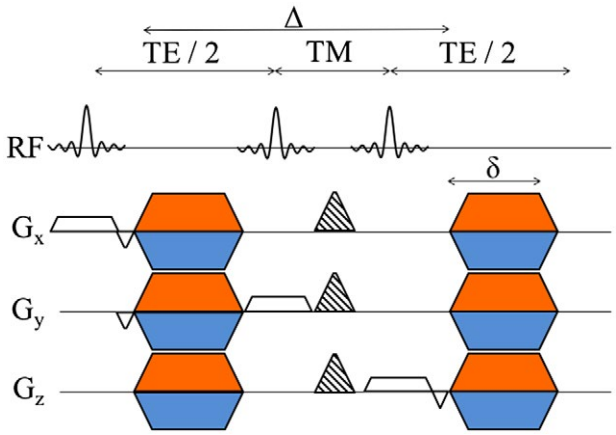

FIGURE 1 DW STEAM MRS sequence: The three 90° slice selective RF pulses generate a stimulated echo in a single voxel. The diffusion gradients (in color) are introduced in a standard STEAM MRS sequence to achieve diffusion weighting. To compensate for eddy current effects, the diffusion-weighting gradients alternate over the acquired averages between positive (orange) and negative (blue) polarity

The preprocessing of the spectra was based on a custom-built processing pipeline implemented in-house in MATLAB (MathWorks, Natick, MA).[17] The pipeline included zero order phase correction of each b-value and polarity and Gaussian apodization. The single averages were frequency aligned by taking the cross-correlation with the first average of each b-value and polarity and shifting the spectrum of the remaining averages in frequency domain until a maximum of the cross-correlation function was obtained. Averages with a deviation of the methylene peak amplitude of more than 2 SDs from the mean methylene peak amplitude were identified as outliers and excluded from the subsequent analysis. The effect of the outlier removal is further discussed in Supporting Information Figure S6 in the supplementary material, which is available online. The remaining averages for both polarities were combined and corrected for eddy currents. Peak area quantification was performed on the real spectrum fitting 8 fat peaks assuming Lorentzian peak shapes. The fat peaks included were: methyl at 0.90 ppm; methylene at 1.30 ppm, β-carboxyl at 1.60 ppm, α-olefinic at 2.02 ppm, α-carboxyl at 2.24 ppm, diallylic methylene at 2.75 ppm, glycerol at 4.20 ppm, and olefinic at 5.29 ppm.[17] Water signal was not detectable due to the strong diffusion-weighting. Only the methylene peak area (at 1.3 ppm) was used to estimate the lipid droplet size, because the different fat peaks, in general, differ in diffusion coefficient[6,15] and T_1 relaxation time.[18]

2.3 | Estimation of the diffusion restriction size

Equation 1 was used for fitting the acquired DW data. The infinite sum was calculated to the ~3000th root because afterward only negligible deviations from the signal decay were observed.

For a given diffusion time, the non-DW signal depends on the diffusion time due to T_1 relaxation effects. This gives the expression:

$$S_0(\Delta) = \rho * \exp\left(-\frac{\Delta - \frac{TE}{2}}{T_1}\right) = \rho * \exp\left(-\frac{TM}{T_1}\right) \quad (3)$$

The TE of the STEAM sequence was kept constant; therefore, no additional T_2 relaxation needed to be considered. The experimental data across diffusion gradient strengths, diffusion gradient durations, and diffusion times S_{exp} were thus fitted to an analytical signal expression using a 4-parameter fit with unknowns the free diffusion constant D, the diameter of diffusion restriction barrier d, the T_1 relaxation constant, and the overall signal ρ:

$$\underset{D,d,T_1,\rho}{\arg\min} \; || \, S(\Delta, \delta, G, T_1) * \rho * exp\left(-\frac{TM}{T_1}\right) - S_{exp} \, || \quad (4)$$

2.4 | Numerical simulations

To evaluate the noise characteristics of the fitting, a Monte Carlo simulation was performed. Rician noise with a SNR between 100 and 1300 was added to an artificial signal decay curve and the apparent diameter of the restriction barrier was fitted. The SNR was defined as the signal amplitude divided by the SD of the signal for the lowest b-value and shortest diffusion time. The simulation was repeated 500 times for each SNR level and both the mean and SD values of the diameter were calculated. The simulation parameters were: TM: between 300 ms and 700 ms in 100 ms steps, $\delta = 28$ ms, b-value = 10,000 – 20,000 – 40,000 – 60,000 s/mm^2 and restriction barrier diameter: 60 μm. The simulation was performed using diffusion coefficient values $D = 0.7 \times 10^{-5}$ mm^2/s and $D = 1.5 \times 10^{-5}$ mm^2/s to account for the dependence of D on the temperature for the phantom and in vivo experiments, respectively (see also below).

In a realistic experimental setting, it is likely that there will be a lipid droplet size distribution found for all lipid droplets. In bone marrow adipocytes, the droplet size distribution was reported to be a Gaussian distribution.[19] To test the dependency of the method on particle size distribution, the apparent diameter was simulated using 3 different lipid droplet sizes and different particle distributions. Here, lipid droplet diameters of 20 μm, 40 μm, and 60 μm were assumed and the theoretical signal assuming a Gaussian diameter distribution with SDs between 0 μm and 10 μm was calculated with the same simulation parameters as in the previous simulations. The simulated signal decay curves were again fitted using Equation 4 (which assumes a single diameter).

2.5 | Phantom measurements

To validate the proposed method water–fat phantoms (oil-in-water emulsions) with high fat concentration closely resembling in vivo adipose tissue lipid content were produced. Each phantom contained 800 mL sunflower oil (ARO), 200 mL soft water, 4 mL Tween 80 (Sigma-Aldrich, Taufkirchen) (emulsifier) and 1 g of sodium benzoate (Roth, Karlsruhe). Emulsification was carried out with a colloid mill (IKA Labor-Pilot 2000/4, IKA-Werke GmbH & Co. KG, Staufen) at 5000, 6000, 9000, and 12,000 revolutions per minute (rpm) to obtain different oil droplet sizes within the water matrix (standardized emulsification process).[20]

The phantoms were scanned on a clinical 3T system (Ingenia Elition, Philips Healthcare, Best) with a maximal diffusion gradient strength of 40 mT/m and a slew rate of 200 mT/m ms using 8-channel wrist coil with the following scanning parameters: DW STEAM MRS with volume of interest: (15 mm)^3, TE: 60 ms, $\delta = 28$ ms, TR: 1800 ms, 4096 points, spectral width: 5000 Hz, 8 phase cycles, 16 averages per b-value (half of the averages with positive and the other half with negative polarity), 1 start-up cycle, b-values: 10,000 – 20,000 – 40,000 – 60,000 s/mm^2, 14:02 min scan time per voxel location, mixing times of 300, 400, 500, 600, and 700 ms. As the DW sequence applied maximum available gradient strength and slew rates, strong vibrations of the scanner table were induced. To minimize any measurement errors induced by the table vibrations, the phantoms were placed on a wooden support table decoupled from the scanning table.

To estimate the SNR of the phantom scans, the measurements were repeated 10 times in the 6000 rpm phantom for the shortest mixing time and lowest b-values. The methylene peak area was estimated individually for each average and the peak area SNR was defined as the mean signal value divided by SD of the methylene peak area.

For validation purposes, the lipid particle size distribution within the water–fat phantoms was measured by 2 different reference methods. First, the lipid droplet size was measured by dynamic light scattering using a particle sizing instrument (Mastersizer 2000 with Hydro 2000S dispersing unit, Malvern Instruments GmbH, Worcestershire). Samples were diluted with 0.5 % sodium dodecyl sulfate (Serva, Heidelberg) solution (1:10, v/v) to separate agglomerates and measure the size of single droplets. Size distributions were logarithmically depicted between 10 nm to 10 mm.

Last, light microscopy was used to analyze the droplet sizes. All the slides were divided into 3 different sections with Leukosilk surgical tape (BSN Medical, Hamburg, Germany) and prewetted with 100 μL water. Afterward, small amounts of emulsion (approximately 10 μL) were added and spread across each section through gentle swirling. The slides were cover-slipped, and 3 images were acquired per section using 20 × magnification (Leica DMI 4000 b, Leica Microsystems, Wetzlar). The droplet area was determined automatically using CellProfiler image analysis software (Broad Institute, Cambridge) and converted to diameter by assuming that lipid droplets were spherical.[21] Between 1725 droplets (5000 rpm emulsion) and 8467 droplets (12,000 rpm emulsion) were automatically measured to determine the particle distributions.

All the reported particle size distributions were based on the lipid droplet volume and not the lipid droplet number. This characterization accounted for the fact that larger lipid droplets contained more lipids. From the particle size distributions, mean diameters were extracted for all the validation experiments and, then, were used subsequently for the analysis.

2.6 | In vivo measurements

Given the strong diffusion weighting and the long diffusion times, the proposed DW-MRS sequence was sensitive to any

kind of macroscopic movement. To eliminate these potential artifact, the proposed method was applied to the nonmoving fatty tissue of the tibia bone marrow.

The robustness in vivo was measured by first scanning the tibia of 3 healthy volunteers 3 times in a row at approximately the same location, with subject repositioning on the scanner table between the 3 scans. To identify location-dependent microstructural differences, the tibia bone marrow of 7 healthy volunteers (27.0 ± 1.8 years old) was scanned at 2 different locations. Water-only images (to aid voxel placement) were computed using the online vendor's chemical shift encoding-based water–fat-separation algorithm on the data from a 3D multi-echo gradient echo sequence using bipolar (non–fly-back) gradient readout. The parameters FOV = 140 × 140 × 105 mm^3, voxel size = 1.35 × 1.35 × 1.5 mm^3, TR/TE1/ΔTE = 8.3/1.31/1.1 ms, flip angle = 5°, and 6 echoes were used for the measurement. The first spectroscopy voxel was placed approximately 1 cm below the growth plate in the tibia bone marrow (proximal location), whereas the second voxel was placed approximately 4 cm below the growth plate (distal location). The repeatability experiment was performed at the proximal location. Both experiments were performed on the same clinical scanner as the phantom experiments and with an 8 channel extremity coil. The sequence parameters were, except of the voxel size (volume of interest of proximal location: 18 × 18 × 18 mm^3; distal volume of interest: 14 × 14 × 20 mm^3), identical with the phantom experiments.

3 | RESULTS

3.1 | Simulation results

In Figure 2, the noise performance of the droplet size estimation was evaluated for phantom and in vivo conditions and at different peak area SNR levels. The experimentally determined methylene peak SNR was also included in Figure 2 for both conditions. The simulation shows that the proposed method leads to an underestimation of the droplet diameter if

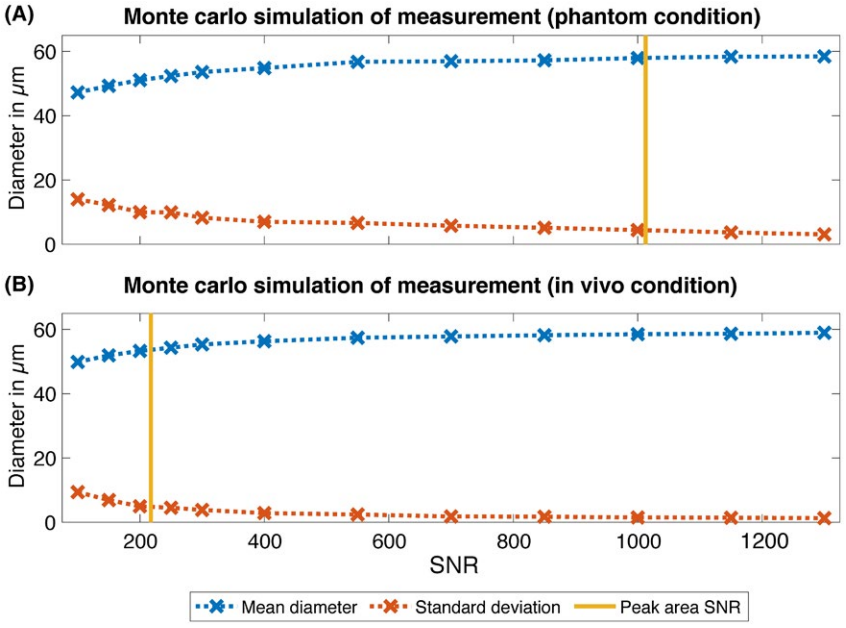

FIGURE 2 Monte Carlo simulation of the droplet size estimation for different peak area SNR levels in (A) phantom and (B) in vivo conditions. The experimentally determined peak area SNR is also shown by the vertical yellow line. A decreased peak SNR leads to an underestimation of the theoretical diameter of 60 μm and a higher SD. The experimentally measured peak SNR has a relative error of 7.6 % (phantom) and 9.3 % (in vivo), respectively

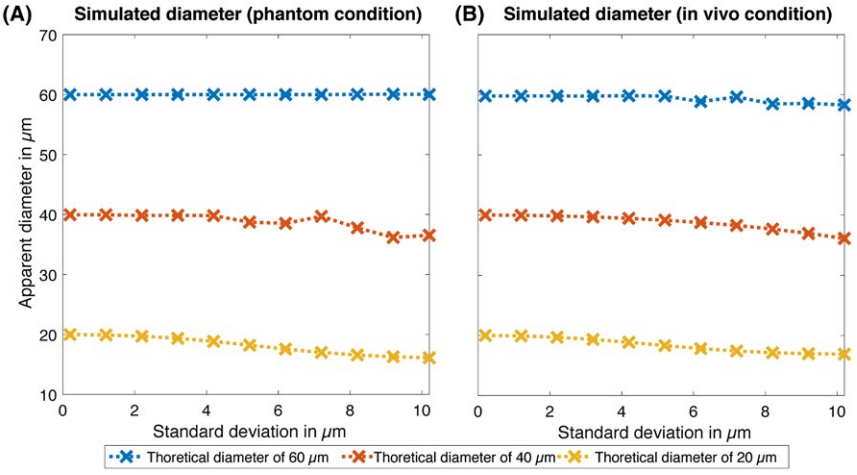

FIGURE 3 The simulation dependence of the proposed method on the lipid droplet size distribution for (A) phantom and (B) in vivo conditions. The lipid droplet diameter stays within a relative error of 11 % (phantom) and 9 % (in vivo), respectively, up to a particle SD of 10 μm for the 3 different theoretical diameters

the peak SNR is low in both the phantom and the in vivo experimental settings. In the phantom case with a lower diffusion constant the dependency of the mean droplet size on the peak area SNR is more prominent. However, the difference between the simulated cell diameter and the real cell diameter is small when a sufficient peak SNR is reached. Using a simulated diameter of 60 μm, an experimental diameter of 58.0 ± 4.4 μm (phantom condition) and 53.3 ± 4.9 μm (in vivo condition) was estimated at the experimentally determined peak area SNR levels.

Figure 3 shows the dependency of the simulated lipid droplet diameter on the Gaussian particle distribution. The error in the droplet diameter estimation was found to stay below 11 % for the phantom condition and 9 % for the in vivo condition when the SD of the distribution was increased to 10 μm. For larger SDs of the droplet distribution, an underestimation of the experimental mean diameter was predominantly observed for the smaller mean diameters of 20 μm and 40 μm.

This robustness in estimating the real mean diameter also in the presence of an underlying particle distribution was observed for all simulated diameters and SDs in both phantom and in vivo conditions.

3.2 | Phantom results

Figure 4 shows representative DW MR spectra and DW signal decay results from the water–fat phantom with a 6000 rpm rotation frequency. The measurement was performed by placing the phantom on the scanner table (Figure 4, first row). The phantom was stabilized on a wooden support table, which helped to decouple the phantom from the MR scanner and reduce the influence of any vibrational artifacts (Figure 4, second row). Both the DW spectra and the fitted signal decay curves for each mixing time were very similar for the 2 experimental conditions. The fitted model and the experimentally acquired data points were both in good agreement. However, when studying the relative signal at the highest b-value, a systematic decrease in the signal with increasing mixing times was observed when the wooden support table was used. When the phantoms were placed on the scanner table also a decrease of the relative signal decay was

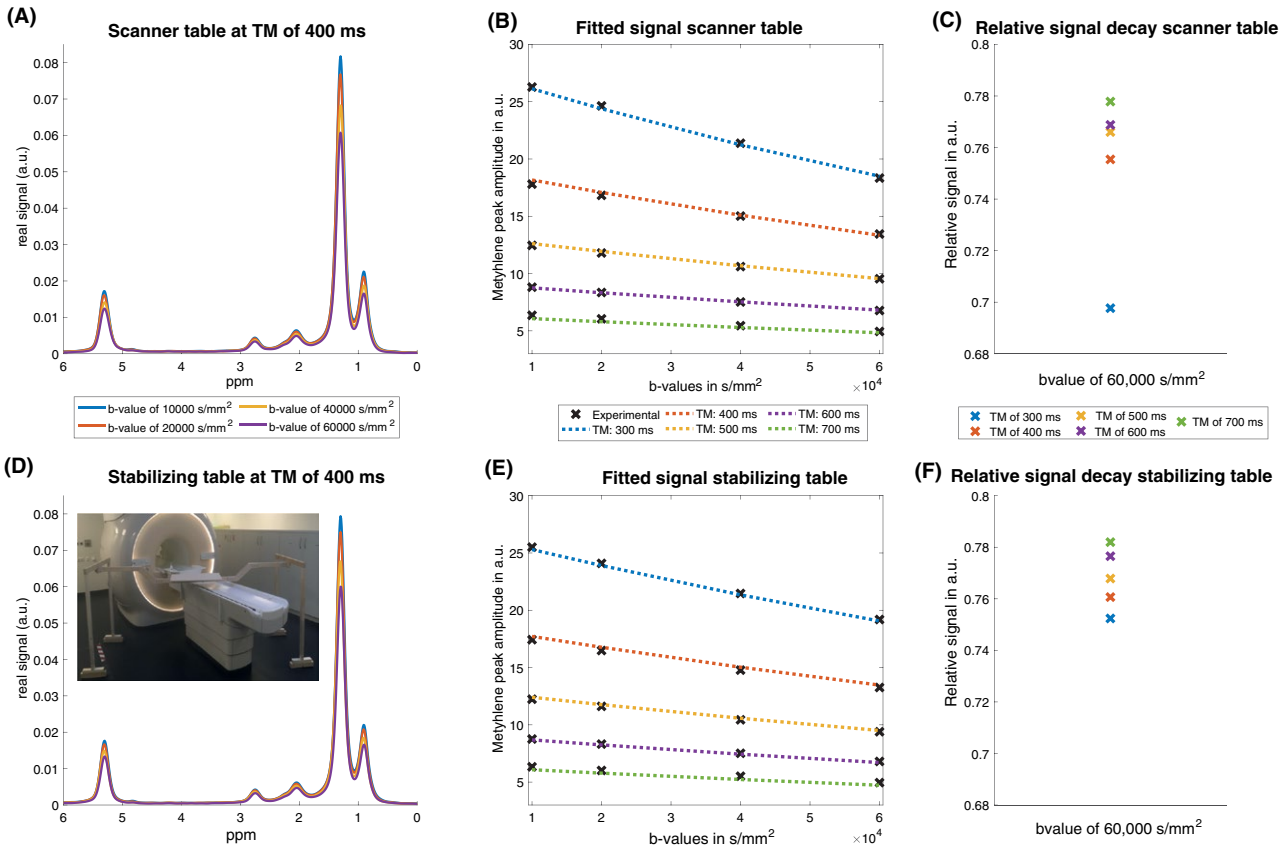

FIGURE 4 DW MR spectra (A,D), fitted methylene peak area signal (B,E) and relative signal decay (signal at the highest diffusion weighting divided by the signal at the lowest diffusion weighting at a given TM) at highest b-value for the 6000 rpm phantom (C,F) measured on the scanner table (first row) and measured on the wooden support table (second row). Minor differences can be observed when comparing the DW spectra and the DW signal decay curves. A systematic and stable decrease of the relative signal decay with increasing diffusion time (as indicated by the theoretical description of restricted diffusion) is only visible when the stabilizing table was used (F), compared with when the samples were placed on the scanner table (C)

visible. However, the diffusion signal decay dependency on the acquired mixing times was irregular, indicating additional confounding factors on the droplet size measurement. A systematic decrease in ADC with increasing diffusion time (as in exemplary case from an ADC of 5.7×10^{-5} mm^2/s to 4.8×10^{-5} mm^2/s when increasing the mixing time from 300 ms to 700 ms) agreed well with the theoretical description of restricted diffusion. The scanning table vibrations could induce additional signal decay, and these artifacts might have been superimposed on the measured signal. Therefore,

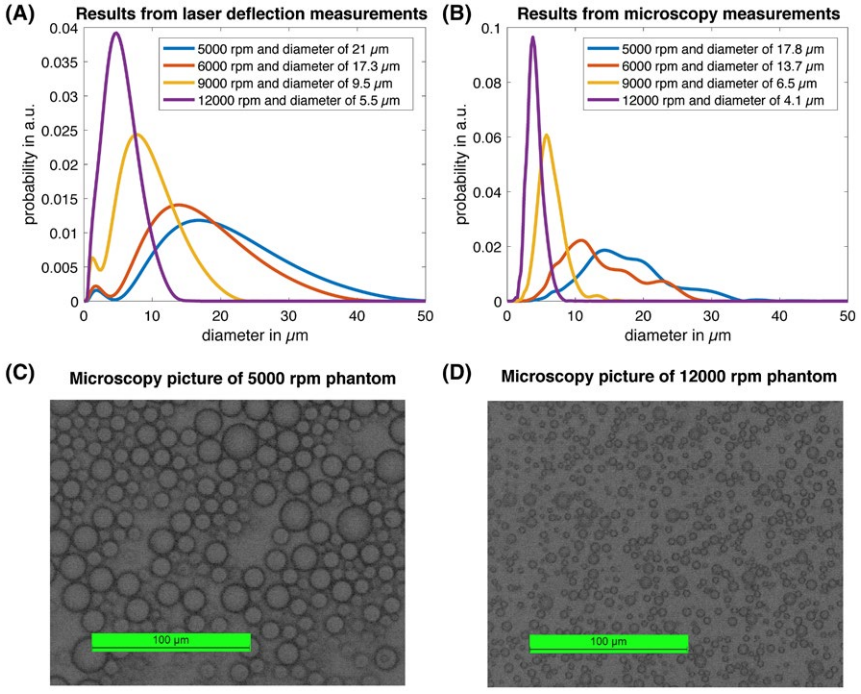

FIGURE 5 The volume particle size distributions in water–fat phantoms measured with (A) laser deflection and (B) microscopy. The distributions measured with both methods show similar shapes. The microscopic analysis measured smaller diameters for all phantoms. The second row shows an image section of the pictures used for the microscopy analysis for (C) the 5000 rpm phantom and (D) the 12,000 rpm phantom

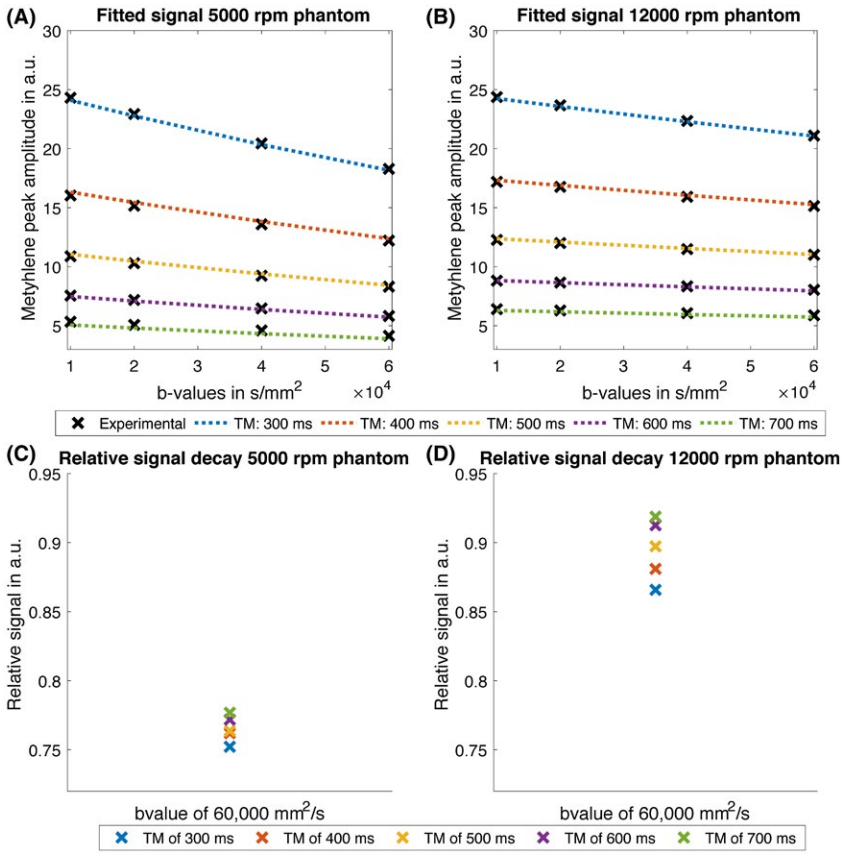

FIGURE 6 Representative signal decay curves and fitting results for (A) the 5000 rpm phantom and (B) the 12000 rpm phantom. C,D, The corresponding relative signal decay, which is the signal at the highest diffusion weighting divided by the signal at the lowest diffusion weighting at different TMs. A decrease in the signal decay slope with increasing diffusion time indicates the presence of diffusion restriction effects. In the 12,000 rpm phantom, a strong dependency of the relative signal decay on the diffusion time is observed and indicates smaller restriction barriers

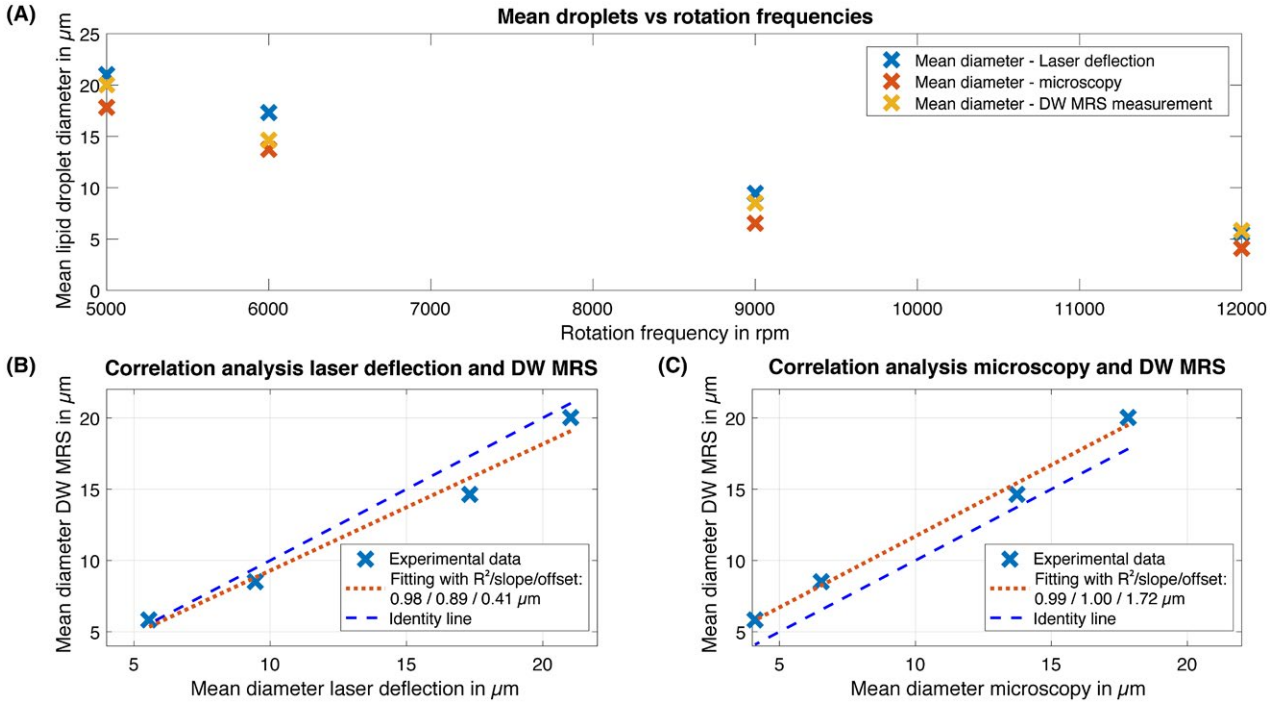

FIGURE 7 The mean diameter obtained by DW-MRS for the 2 validation measurements (A). The DW-MRS correlation analysis using (B) laser deflection and (C) microscopy are also shown. The R^2 coefficients are in good agreement between DW-MRS and laser deflection ($R^2 = 0.98$; $P = 0.01$) and between DW-MRS and microscopy ($R^2 = 0.99$; $P < 0.01$)

the subsequent phantom scans were all performed with the wooden support table. The quality of the MR data for the other phantoms was similar to the data shown in Figure 4.

Figure 5 shows the particle size distributions obtained using laser deflection (Figure 5A) and microscopy analysis (Figure 5B). Based on the mean diameter distributions, values were extracted for each phantom. The particle size distributions measured with both methods showed, in general, a similar shape. The extracted mean diameters for the 5000, 6000, 9000, and 12000 rpm phantoms were 21 μm, 17.3 μm, 9.5 μm, and 5.5 μm (laser deflection measurement) and 17.8 μm, 13.7 μm, 6.5 μm, and 4.1 μm (microscopy measurement). In general, both methods showed the same trend. However, the mean diameters obtained using microscopy were found to be smaller than the diameters measured by laser deflection.

Figure 6 shows a comparison between the signal decay curves of the phantom with a stirring frequency of 5000 rpm and 12,000 rpm, respectively. In both phantoms, the experimental signals and the fitted signals were in good agreement with each other. Nevertheless, the difference between the 2 phantoms were not easily discernable on the pure signal decay curves for the different mixing times, except a stronger signal decay of the 5000 rpm phantom. The relative signal decay at the highest b-value revealed that it was slower for the 12,000 rpm phantom compared with the 5000 rpm phantom for all measured mixing times. A dependency on the mixing time was found more prominent for the 12,000 rpm phantom.

Figure 7A compares the mean diameter obtained by DW-MRS, laser deflection, and microscopy for the different water–fat phantoms. All 3 measurements showed the same trend of reduced lipid droplet size with increasing stirring rotation frequency. In Figure 7B and E, the lipid droplet size estimated by DW-MRS, laser deflection (Figure 7B), and microscopy (Figure 7C) are shown. The coefficients of determination for the linear regression were high when comparing DW-MRS with laser deflection ($R^2 = 0.98$; $P = 0.01$) and DW-MRS with microscopy ($R^2 = 0.99$; $P < 0.01$). The resulting linear regression showed a slope of 0.89 and an offset of 0.41 μm when comparing DW-MRS measurements with the laser deflection. A slope of 1.00 and an offset of 1.72 μm was found when comparing DW-MRS and microscopy measurements.

3.3 | In vivo results

Figure 8 shows the spectroscopy voxel placement, the in vivo tibia bone marrow DW spectra for the shortest mixing time and the fitted signal decay curves for the proximal voxel location (first row) and distal voxel location (second row) from one volunteer. Here, the DW signal had a higher attenuation when comparing the in vivo measurements with the phantom measurements. The acquired spectra and signal decay curves were of similar quality for all measurements taken. Based on the extracted peak area for methylene, the size of the bone

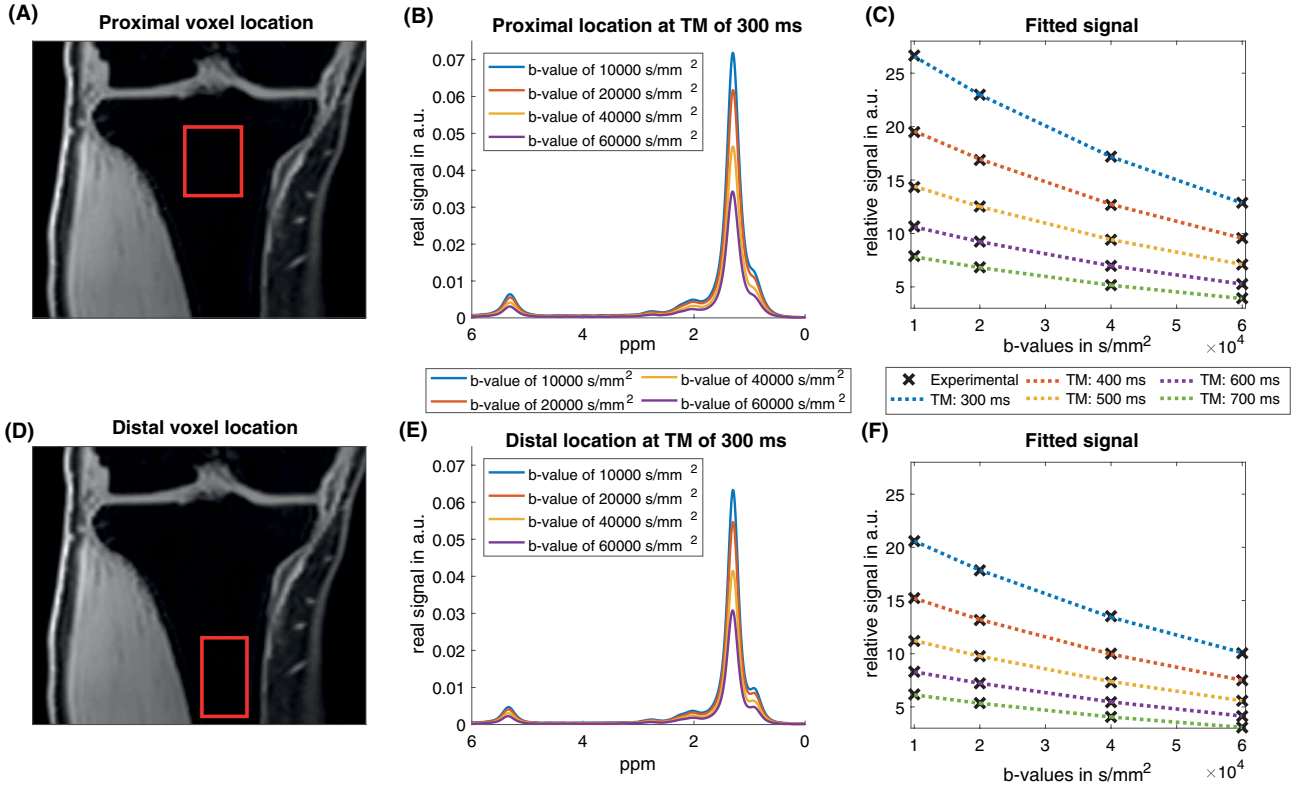

FIGURE 8 The voxel location in water-only Dixon images of the tibia at the A, proximal and (D) distal location. B,E, The DW spectra at the shortest TE. C,F, The corresponding fit to the peak area of methylene. The fitted signal decay curves correspond well to the measured data points

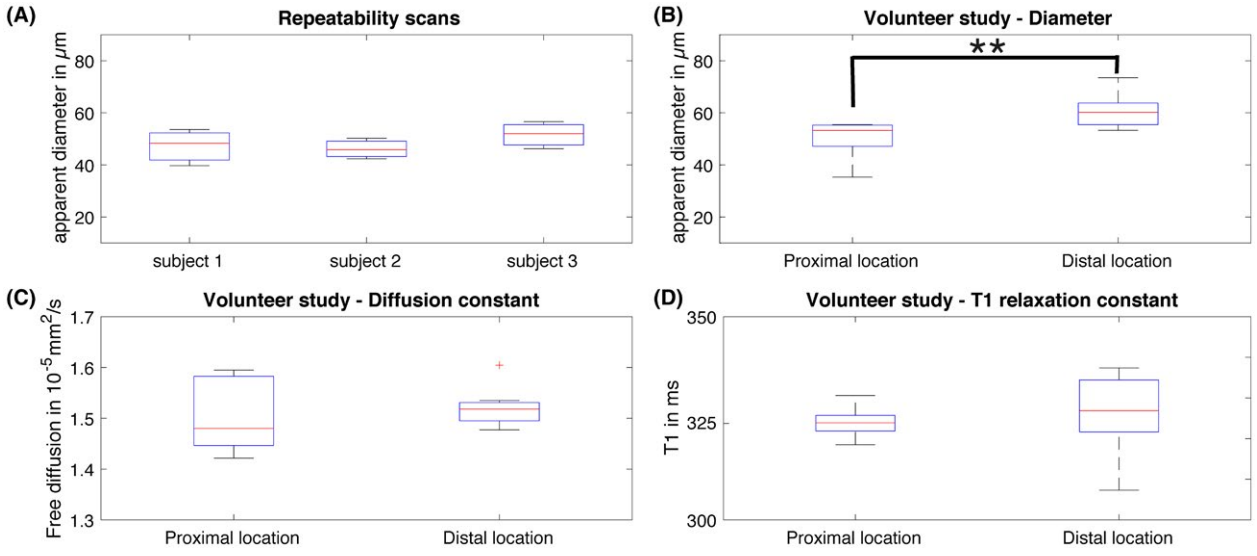

FIGURE 9 A, A summary of the repeatability measurements in the 3 subjects. The mean adipocyte cell diameter stayed within a relative error of 15% in all cases. The mean diameters measured for the repeatability study were 47.2 ± 7.0 μm, 46.1± 4.0 μm, and 51.6 ± 5.2 μm. B, A boxplot from the volunteer study. For every volunteer, the cell diameter was significantly larger in the distal location (61.1 ± 6.8 μm) compared with the proximal location (50.1 ± 7.3 μm) ($P = 0.003$). The free diffusion constant (C), and T_1 relaxation constant (D) for the volunteer study did not show significant differences between the two locations

marrow adipocytes was estimated for both locations and in all subjects. The fitting and the experimental data were also in good agreement.

Figure 9A shows the results from the in vivo repeatability scans. The acquired data for the 3 subsequent scans were all processed with the same postprocessing pipeline

and the mean diameter for the bone marrow adipocytes size was extracted. The coefficient of variation (defined by the SD divided by the mean value) stayed below 15 % for all 3 volunteers studied, with a mean coefficient of variation of 11.5 %.[22] The measured diameters for each of the 3 volunteers were 47.2 ± 7.0 μm, 46.1 ± 4.0 μm, and 51.6 ± 5.2 μm.

Figure 9B summarizes the results from the volunteer study at 2 different locations in the tibia. Larger lipid droplet sizes were observed more distally in the tibia bone marrow. The mean diameter at the proximal location was 50.1 ± 7.3 μm and 61.1 ± 6.8 μm at the distal location. For each volunteer, the diameter measured distally was smaller than the diameter measured proximally. A significant difference was found between the two locations ($P < 0.01$).

4 | DISCUSSION

The present study proposes a methodology to measure lipid droplet sizes with DW-MRS. The restricted diffusion effects in the DW-MR measurements of lipid droplets have been reported previously for lipid droplets a few microns in size using the strong gradient hardware of preclinical MR scanners.[14,15] The diffusion restriction effect induced by the lipid droplet boundary on the fat DW signal is reduced as the lipid droplet size increases, requires longer TEs as the gradient strength of gradient hardware decreases and can be confounded by scanner table vibrations and physiological motion due to the need of using high b-values. The present results show that it is feasible to measure large lipid droplet size using the gradient hardware of a clinical 3T system based on both phantom and in vivo measurements.

Previously published work has predominantly extracted an estimate for the restriction size by exploiting deviations from the monoexponential diffusion signal decay curve at a specific diffusion time.[14,15] An estimate for the diffusion restriction size can also be obtained when investigating the dependency of the diffusion constant on the diffusion time[23] assuming the short diffusion time limit (mean free path length is much smaller than the restriction barrier size). Instead, in the present work, signal decay curves obtained at different mixing times (corresponding to different diffusion times) are fitted all at once using the signal model of Equation 4. The present approach additionally requires the fitting for the T_1 relaxation constant because the signal decay curves acquired at different mixing times yield different T_1 weighting. The Supplementary Material characterizes the superior noise performance of the present single-step fitting approach compared with a 2-step approach first estimating ADC per diffusion time and second fitting the ADC dependence on diffusion time to a diffusion model (see Supporting Information Figure S1-S5).

The simulations performed showed that it is possible to extract information about the restriction barrier size when the peak SNR is sufficient. The effect of the diffusion restricting barriers on the DW signal decay curve is small compared with the influence of the diffusion properties or relaxation parameters. Therefore, a rather high peak area SNR is necessary to extract reliable information about the restricting barrier dimensions. However, for both the phantom and in vivo conditions, the experimental parameters were set so a reliable estimate of the droplet size could be measured. The simulated error stayed below 7.6 % for the phantom measurements and below 9.3 % for the in vivo measurements. If the peak area SNR is low, real lipid droplet size can be underestimated because the noise floor at longer mixing times mimics stronger diffusion restriction effects. Based on the simulations and the experimentally obtained in vivo peak SNR values, it can be inferred that the bone marrow adipocytes size will be underestimated. Improvements in the experimental setup and longer scan times may help to overcome such problems.

Another important aspect of the estimated lipid droplet size is the lipid droplet distribution. Figure 3 indicates that an underlying Gaussian particle distribution will only result in small deviations from the real mean value even if the distribution is broad compared with the cell diameter (e.g., an SD of 10 μm and a mean diameter of 20 μm). This finding is important for 2 reasons. First, the current description of the restricted diffusion behavior of the signal only assumes a single diameter. Multiple radii or a distribution of particle sizes can be introduced to the model but, given a high peak SNR is required, introducing more fitting parameters would only decrease the stability of the fitting process. Second, in biological tissue, a particle size distribution is more likely than a single defined diameter. Given the shown robustness of the proposed method toward the particle distribution broadness, it can be concluded that the present method delivers meaningful mean droplet sizes even if no particle size distribution is considered in the modelling, at least under the assumption of an underlying Gaussian distribution.

The analysis of water–fat phantoms was of particular interest because a ground-truth particle size was obtained through 2 independent validation measurements. Moreover, lipid droplets in a liquid water matrix can be considered as a good model to examine the restriction effects in fat adipocytes. The phantom lipid droplet size distributions measured using laser deflection and microscopy (Figure 5) were found to be quite similar. Due to the manufacturing process, a decrease in the stirring frequency of the colloid mill leads to larger lipid droplet size distributions. The observed differences between the 2 validation measurements could be explained due to the structural inhomogeneity of the water–fat phantoms, measurement inaccuracy, and differences in the phantom material used during the preprocessing stage. The

trend toward smaller diameters measured using the microscopy technique could also partly explain the fact that light scattering only measured the outer diameter of the lipid droplets, whereas microscopy postprocessing software typically measures the inner diameter.

When examining the water–fat phantoms with DW-MRS, vibrations from the scanner table were observed due to the strong diffusion weighting gradients. Figure 4 highlights the need to decouple the samples from the scanner table. If no auxiliary hardware is used and the samples are directly placed onto the scanning table, excess signal attenuation is observed at specific mixing times. This could be explained by certain mechanical resonances that cause the scanner table to vibrate at specific sequence times and diffusion gradient strengths.[24] Consequently, the signal decay cannot be described by a model of restricted diffusion, because the scanner table vibrations induce deviations from such a model. A wooden support table that is not connected to the scanner and, therefore, decoupled from the vibrations mitigated the vibration-induced artifacts. Therefore, all the phantoms were examined with this additional hardware.

In general, as Figure 4 shows, the peak SNR found in DW spectra was very high for all phantoms and mixing times. Phantoms manufactured with increased stirring frequency showed a stronger dependence on the signal decay when different mixing times were applied to the DW-MRS sequence. That corresponds to a stronger dependency of the apparent diffusion constant on the diffusion time for smaller diffusion restriction barriers. In Figure 6, this stronger dependency of the relative DW signal decay on the diffusion time can be observed for the phantom with the smallest lipid droplet diameter (12,000 rpm phantom) compared with the phantom with the largest lipid droplet diameter (5000 rpm phantom). For all the 4 different water–fat phantoms, a mean lipid droplet diameter was extracted and compared with the 2 validation measurements. For lipid droplet sizes obtained by DW-MRS, both validation measurements resulted in high R^2 values. Therefore, the present water–fat phantom study shows that DW-MRS can measure the mean lipid droplet diameters with small absolute deviations found between the different measurement methods. These results prove the applicability of the proposed method to measure lipid droplet sizes in water–fat containing phantoms.

In vivo, the presented method showed good reproducibility. The measured bone marrow diameter stayed within a relative error of 15 % during the re-positioning experiments for all the 3 healthy volunteers. This shows that the present approach is capable of measuring lipid droplet size with good precision. In the volunteer study, the bone marrow adipocytes were found to have a diameter between 40 and 70 μm, showing a tendency for larger cells more distally in the tibia bone marrow. Diameters of around 60 μm were reported in previous studies for bone marrow adipocytes,[19] and recent findings indicate that they also increase in size from proximal to distal locations.[4] Therefore, the presently extracted adipocyte sizes are consistent with the literature and the observed differences along the long axis of the tibia agree with recent reports.

The noninvasive measurement of lipid droplet size has a wide range of applications in different tissues. In bone marrow, MR techniques have been emerging for measuring bone marrow water-fat composition[10] but techniques are lacking for the assessment of bone marrow adipose tissue (BMAT) microstructure, which is needed to differentiate between regulated BMAT and constitutive BMAT.[4] In human adipose tissue depots containing brown adipose tissue, techniques assessing lipid droplet microstructure are needed to overcome the partial volume effects on the fat fraction measurements in regions containing both white and brown adipose tissue.[25,26] The present results show that lipid droplet size measurements can be validated in water–fat phantoms and applied with good reproducibility in the tibial bone marrow. However, any extension to the present methods for other body regions requires further investigation.

The methodology shown in this study has several limitations. First, only the mean lipid droplet diameter can be estimated. The results from the simulations and phantom study show that deviations of the apparent lipid droplet diameter from the real lipid droplet diameter can occur. However, the deviations from the mean droplet diameter size were relatively small for a range of possible droplet diameters and different Gaussian droplet size distributions. Second, the range in droplet size for the water–fat phantoms scanned did not match the expected adipocytes size within the bone marrow or other larger adipocytes. However, good agreement was shown for the range of phantom diameters useed. It can be assumed that this will also be valid for larger lipid droplets if the appropriate peak SNR requirements are met. Third, no validation measurements for the in vivo adipocyte cell diameter was performed due to a lack of noninvasive reference measurements. However, the phantom data obtained did show a good agreement with 2 different reference measurements. The in vivo extracted bone marrow adipocyte size is consistent with those in literature and the observed differences along the axis of the tibia also agree with recent reports.[4,19] Fourth, no optimization of the experimental parameters to reduce the total acquisition time was performed in the present work. Finally, a translation of the presented method to anatomical regions with macroscopic physiological motion (induced by the respiratory or the cardiac cycle) is challenging due to the strong diffusion weightings and long diffusion times. Triggering and smaller voxel sizes could help to decrease the effects of intravoxel dephasing due to macroscopic physiological movement.

5 | CONCLUSIONS

In summary, the methods used in this study were able to probe diffusion restriction effects in lipid droplets in phantoms and in vivo at a 3T clinical scanner using long diffusion time and high b-value DW-MRS and to estimate lipid droplet size. The presented method was validated in phantoms showing good agreement with laser deflection and light microscopy measurements. The application of the method in the in vivo tibial bone marrow of healthy volunteers showed an estimation of the lipid droplet size with good repeatability and in agreement with the literature.

ACKNOWLEDGMENTS

The present work was supported by the European Research Council (grant agreement No 677661, ProFatMRI). This work reflects only the authors view and the EU is not responsible for any use that may be made of the information it contains. The authors would also like to acknowledge research support from Philips Healthcare.

REFERENCES

1. Suzuki M, Shinohara Y, Ohsaki Y, Fujimoto T. Lipid droplets: size matters. *J Electron Microsc (Tokyo)*. 2011;60(Suppl 1):S101–S116.
2. Cousin B, Cinti S, Morroni M, et al. Occurrence of brown adipocytes in rat white adipose tissue: molecular and morphological characterization. *J Cell Sci*. 1992;103(Pt 4):931–942.
3. Salans LB, Cushman SW, Weismann RE. Studies of human adipose tissue. Adipose cell size and number in nonobese and obese patients. *J Clin Invest*. 1973;52:929–941.
4. Scheller EL, Doucette CR, Learman BS, et al. Region-specific variation in the properties of skeletal adipocytes reveals regulated and constitutive marrow adipose tissues. *Nat Commun*. 2015;6:7808.
5. Assaf Y, Blumenfeld-Katzir T, Yovel Y, Basser PJ. AxCaliber: a method for measuring axon diameter distribution from diffusion MRI. *Magn Reson Med*. 2008;59:1347–1354.
6. Lehnert A, Machann J, Helms G, Claussen CD, Schick F. Diffusion characteristics of large molecules assessed by proton MRS on a whole-body MR system. *Magn Reson Imaging*. 2004;22:39–46.
7. Steidle G, Eibofner F, Schick F. Quantitative diffusion imaging of adipose tissue in the human lower leg at 1.5 T. *Magn Reson Med*. 2011;65:1119–1125.
8. Jezzard P, Barnett AS, Pierpaoli C. Characterization of and correction for eddy current artifacts in echo planar diffusion imaging. *Magn Reson Med*. 1998;39:801–812.
9. Anderson. Analysis and correction of motion artifacts in diffusion weighted imaging. *Magn Reson Med*. 1994;32:379–387.
10. Karampinos DC, Ruschke S, Dieckmeyer M, et al. Quantitative MRI and spectroscopy of bone marrow. *J Magn Reson Imaging*. 2018;47:332–353.
11. Nicolay K, Braun KP, Graaf RA, Dijkhuizen RM, Kruiskamp MJ. Diffusion NMR spectroscopy. *NMR Biomed*. 2001;14:94–111.
12. Ronen I, Valette J. Diffusion-weighted magnetic resonance spectroscopy. *eMagRes*. 2015;4:733–750.
13. Brandejsky V, Kreis R, Boesch C. Restricted or severely hindered diffusion of intramyocellular lipids in human skeletal muscle shown by in vivo proton MR spectroscopy. *Magn Reson Med*. 2012;67:310–316.
14. Cao P, Fan SJ, Wang AM, et al. Diffusion magnetic resonance monitors intramyocellular lipid droplet size in vivo. *Magn Reson Med*. 2015;73:59–69.
15. Verma SK, Nagashima K, Yaligar J, et al. Differentiating brown and white adipose tissues by high-resolution diffusion NMR spectroscopy. *J Lipid Res*. 2017;58:289–298.
16. Murday JS, Cotts RM. Self-diffusion coeffcient of liquid lithium. *J Chem Phys*. 1968;48:4938.
17. Ruschke S, Kienberger H, Baum T, et al. Diffusion-weighted stimulated echo acquisition mode (DW-STEAM) MR spectroscopy to measure fat unsaturation in regions with low proton-density fat fraction. *Magn Reson Med*. 2016;75:32–41.
18. Hamilton G, Smith DL Jr, Bydder M, Nayak KS, Hu HH. MR properties of brown and white adipose tissues. *J Magn Reson Imaging*. 2011;34:468–473.
19. Rozman C, Reverter JC, Feliu E, Berga L, Rozman M, Climent C. Variations of fat tissue fraction in abnormal human bone-marrow depend both on size and number of adipocytes - a stereologic study. *Blood*. 1990;76:892–895.
20. Guilmineau F, Kulozik U. Influence of a thermal treatment on the functionality of hen's egg yolk in mayonnaise. *J Food Eng*. 2007;78:648–654.
21. Carpenter AE, Jones TR, Lamprecht MR, et al. Cell Profiler: image analysis software for identifying and quantifying cell phenotypes. *Genome Biol*. 2006;7:R100.
22. Gluer CC, Blake G, Lu Y, Blunt BA, Jergas M, Genant HK. Accurate assessment of precision errors - how to measure the reproducibility of bone densitometry techniques. *Osteoporosis Int*. 1995;5:262–270.
23. Mitra PP, Sen PN, Schwartz LM. Short-time behavior of the diffusion-coefficient as a geometrical probe of porous-media. *Phys Rev B Condens Matter*. 1993;47:8565–8574.
24. Gallichan D, Scholz J, Bartsch A, Behrens TE, Robson MD, Miller KL. Addressing a systematic vibration artifact in diffusion-weighted MRI. *Hum Brain Mapp*. 2010;31:193–202.
25. Hu HH. Magnetic resonance of brown adipose tissue: a review of current techniques. *Crit Rev Biomed Eng*. 2015;43:161–181.
26. Karampinos DC, Weidlich D, Wu M, Hu HH, Franz D. Techniques and applications of magnetic resonance imaging for studying brown adipose tissue morphometry and function. *Handb Exp Pharmacol*. 2018.

SUPPORTING INFORMATION

Additional supporting information may be found online in the Supporting Information section at the end of the article.

FIGURE S1 Alternative assessment of the 1st repetition of the reproducibility scans in subject 3. Signal decay curves for each mixing time with corresponding exponential fitting of the apparent diffusion constant are shown. The dependency of the diffusion constant on the diffusion time is shown in the lower right corner and yields a restriction barrier diameter of 40.88 μm

FIGURE S2 Alternative assessment of the 2nd repetition of the reproducibility scans in subject 3. Signal decay curves for each mixing time with corresponding exponential fitting of the apparent diffusion constant are shown. The dependency of the diffusion constant on the diffusion time is shown in the lower right corner and yields a restriction barrier diameter of 50.41 μm

FIGURE S3 Alternative assessment of the 3rd repetition of the reproducibility scans in subject 3. Signal decay curves for each mixing time with corresponding exponential fitting of the apparent diffusion constant are shown. The dependency of the diffusion constant on the diffusion time is shown in the lower right corner and yields a restriction barrier diameter of 36.66 μm

FIGURE S4 Monte Carlo simulation of the droplet size estimation for different peak area SNR levels in (A) phantom and (B) in vivo conditions. The calculations were performed with fitting Equation S1 proposed by Zielinski et al. The experimentally determined peak area SNR is also shown by the vertical yellow line. A decreased peak SNR leads a higher SD. The dependency of the mean estimated diameter on the SNR is different for the in vivo and phantom cases and there seems to be a systematic offset between the theoretical diameter of 60 μm and the obtained values by the fitting

FIGURE S5 Comparison of the SD of the fitting by the 2-step approach using the model of Zielinski and by the single-step approach using the model of Murday and Cotts. In general, the SD is lower when using the full model of Murday and Cotts compared with Zielinski for the phantom and the in vivo case

FIGURE S6 Effect of the outlier removal on the results of the reproducibility analysis. When no outlier removal is performed, the SD of the apparent measured diameter is greatly increased

How to cite this article: Weidlich D, Honecker J, Gmach O, et al. Measuring large lipid droplet sizes by probing restricted lipid diffusion effects with diffusion-weighted MRS at 3T. *Magn Reson Med*. 2019;81:3427–3439. https://doi.org/10.1002/mrm.27651